

Article

# Microwave-Assisted Photocatalytic Degradation of Organic Pollutants via CNTs/TiO<sub>2</sub>

Yuqing Ren <sup>†</sup>, Yao Chen <sup>†</sup>, Qinyu Li <sup>†</sup>, Hexing Li <sup>\*</sup> and Zhenfeng Bian <sup>\*</sup>

MOE Key Laboratory of Resource Chemistry and Shanghai Key Laboratory of Rare Earth Functional Materials, Shanghai Normal University, Shanghai 200234, China

<sup>\*</sup> Correspondence: hexing-li@shnu.edu.cn (H.L.); bianzhenfeng@shnu.edu.cn (Z.B.)<sup>†</sup> These authors contributed equally to this work.

**Abstract:** Introducing microwave fields into photocatalytic technology is a promising strategy to suppress the recombination of photogenerated charge carriers. Here, a series of microwave-absorbing photocatalysts, xCNTs/TiO<sub>2</sub>, were prepared by combining titanium dioxide (TiO<sub>2</sub>) with carbon nanotubes (CNTs) using a typical alcoholic thermal method to study the promotion of microwave-generated thermal and athermal effects on the photocatalytic oxidation process. As good carriers that are capable of absorbing microwaves and conducting electrons, CNTs can form hot spots and defects under the action of the thermal effect from microwaves to capture electrons generated on the surface of TiO<sub>2</sub> and enhance the separation efficiency of photogenerated electrons (e<sup>-</sup>) and holes (h<sup>+</sup>). Excluding the influence of the reaction temperature, the athermal effect of the microwave field had a polarizing effect on the catalyst, which improved the light absorption rate of the catalyst. Moreover, microwave radiation also promoted the activation of oxygen molecules and hydroxyl groups on the catalyst surface to generate more reactive oxygen radicals. According to the mechanism analysis, the microwave effect significantly improved the photocatalytic advanced oxidation process, which lays a solid theoretical foundation for practical application.

**Keywords:** photocatalysis; microwave; degradation; xCNTs/TiO<sub>2</sub>

**Citation:** Ren, Y.; Chen, Y.; Li, Q.; Li, H.; Bian, Z. Microwave-Assisted Photocatalytic Degradation of Organic Pollutants via CNTs/TiO<sub>2</sub>. *Catalysts* **2022**, *12*, 940. <https://doi.org/10.3390/catal12090940>

Academic Editor: Ewa Kowalska

Received: 4 August 2022

Accepted: 22 August 2022

Published: 24 August 2022

**Publisher's Note:** MDPI stays neutral with regard to jurisdictional claims in published maps and institutional affiliations.



**Copyright:** © 2022 by the authors. Licensee MDPI, Basel, Switzerland. This article is an open access article distributed under the terms and conditions of the Creative Commons Attribution (CC BY) license (<https://creativecommons.org/licenses/by/4.0/>).

## 1. Introduction

As is well known, photocatalysis is a green, environmentally friendly, and low-cost pollution treatment technology. To improve the efficiency of photocatalytic degradation, researchers have usually modified the photocatalyst to reduce the photogenerated electron-hole recombination rate [1–3]. On this basis, by introducing external fields such as microwave fields, the mineralization efficiency of pollutants can be further improved. Recently, microwave (MW) radiation has widely been used in the field of photocatalysis due to its special thermal effect [4–8]. Under the action of the microwave field, the substance is heated from the inside out, which makes the catalyst evenly heated. Thus, microwave-enhanced non-homogeneous class photocatalytic processes have exhibited stronger oxidation performance and significant pollutant degradation ability [9,10]. In addition, the athermal effects of microwaves are also of great benefit to the catalytic process. Microwave fields have a directional alignment effect on polar molecules, stabilizing the transition state of polar reactions and reducing the activation energy, thus accelerating the reactions. Most studies have demonstrated the power of microwaves, but the key roles of the two effects of microwaves in the photocatalytic degradation process have not yet been articulated and are worthy of more attention.

Recently, researchers have further advanced microwave photocatalytic research. Vithal et al. studied the effects of the use of microwaves, photocatalysis, and sequential combinations of microwaves and photocatalysis on bright green dyes. In the case of zinc oxide as a catalyst, the maximum degradation rate obtained by the combination of microwave and photocatalysis is 94.3 ± 0.8% [11]. This suggests that microwaves have

indeed improved in the field of photocatalytic degradation. Arati J et al. studied 4-chloro-2-aminophenol (4C2AP) using different methods based on microwave (MW) irradiation, photocatalysis, and a combination of MW and photocatalytic sequences. When hydrogen peroxide ( $H_2O_2$ ) was used as an additive to enhance degradation, the maximum degradation rate of 4C2AP was 93.23% [12]. Khang et al. synthesized nano-hybrid  $TiO_2/CNT$  materials using hydrolysis. Compared to pure  $TiO_2$  or CNT nanoparticles, nano-mixed  $TiO_2/CNT$  materials exhibited higher catalytic activity when degrading methylene blue (MB) or methylene orange (MO), but the reaction took about 4 h to completely degrade [13]. From this point of view, although microwaves can effectively improve the degradation performance of photocatalytic pollutants, the key mechanism is not clear.

The promotion of microwave photocatalysis can be better understood by choosing a classical catalyst system. As an ideal photocatalyst, titanium dioxide ( $TiO_2$ ) has widely been used due to its lack of toxicity, good chemical stability, and low cost [14,15]. However,  $TiO_2$  often needs to be modified due to its large intrinsic band gap [16–19]. The good electrical conductivity of carbon materials promotes their use in the optimization of photocatalysts, among which carbon nanotubes (CNTs) have a high specific surface area and excellent microwave absorption ability [20–24]. It has been found that CNTs can increase the exciton lifetime because the heterojunction formed at the  $xCNTs/TiO_2$  interface allows for the effective separation of excitons, which enhances their light absorption [25,26]. Given this, with  $TiO_2$  as the representative photocatalyst and CNTs as the microwave absorbers, it was expected that the  $xCNTs/TiO_2$  catalyst could be used to explore the reaction mechanism of the microwave photocatalytic system.

In this work, we investigated the reaction mechanism of the microwave-assisted photocatalytic degradation of organic pollutants in the conditions of UV light and microwave radiation. The microwave photocatalyst,  $xCNTs/TiO_2$ , prepared using the alcoholic thermal method, showed a better methyl orange (MO) degradation performance than that of  $TiO_2$ . By adjusting the reaction temperature and microwave power, the differences in and advantages of the microwave thermal effect and non-thermal effect were further analyzed. This led to a series of theoretical rationales for microwave-assisted photocatalytic degradation, making it a promising strategy for advanced oxidation.

## 2. Results and Discussion

In general, the surfaces of CNTs are relatively smooth and difficult to attach  $TiO_2$  nanoparticles to, so they need to be acidified. The morphology of the acidified CNTs (ACNTs) did not change significantly, but the  $-OH$  and  $-COOH$  groups on their surfaces increased, which was favorable for binding with  $TiO_2$  (Figures S1–S3). Next, different contents of  $TiO_2$  were generated in situ on the pretreated CNTs using an alcoholic thermal method. Transmission electron micrographs (TEMs) show that the  $TiO_2$  was spherical with a diameter of about 150 nm, with CNTs passing through the middle of the nanoparticles (Figure 1a,b). With the increase in the  $TiO_2$ , the CNTs were gradually encapsulated (Figure S4). Elemental analysis indicated that the as-prepared catalyst was composed of three elements: Ti, O, and C (Figure 1c). The structure of the catalytic material was further investigated using X-ray diffraction, and the results show that the peak of the  $xCNTs/TiO_2$  corresponded to anatase ( $2\theta = 25.4^\circ, 37.8^\circ, 48.1^\circ, 53.9^\circ$ ). In addition, the diffraction peak intensity of the anatase increased with the increase in  $TiO_2$ . Furthermore, the addition of CNTs also expanded the absorption of  $TiO_2$  in the visible light region, which provided a good light-harvesting ability for the photocatalytic reaction (Figure 1e).

Taking the common pollutant MO as the active exploration object, it was found that the loading of  $TiO_2$  was not as high as possible (Figure 2a). When the  $TiO_2$  loading was 15, the catalyst showed the optimal degradation rate under the microwave (MW) photocatalytic (UV) synergy (Figure 2b). The photocurrent reflects the separation ability of the photogenerated electron-hole pairs. With the increase in the doping of the CNTs, the difference in the photocurrent increased when the light was turned on and off, as did the separation efficiency of the photogenerated carriers. In addition, the relative size of the arc

radius on the Nyquist diagram corresponds to the size of the charge transfer resistance and the separation efficiency of the photogenerated electron-hole pairs [27,28]. The smaller the arc radius of the impedance spectrum, the better the electron-hole separation. The reason the arc radius changed with different doping amounts of CNTs was the interfacial charge transfer between the CNTs and TiO<sub>2</sub>. The effective charge transfer had the potential to limit electron-hole complexation, which led to a stronger photogenerated electron-hole separation effect. Interestingly, the transient photocurrent response results did not match the activity: the lower the TiO<sub>2</sub> loading was, the higher the photocurrent density was, indicating that the CNTs promoted the separation of photogenerated charges on the TiO<sub>2</sub> (Figure 2c,d). It is worth noting that the photogenerated carriers on the TiO<sub>2</sub> provided only part of the photocatalytic degradation activity during the mineralization process, and the microwave effect brought by the CNTs also played an important role. Therefore, we optimized the 15CNTs/TiO<sub>2</sub> catalyst and used it as the main catalyst to explore the mechanistic process. First, the alcohol heating temperature and time in the preparation process were optimized, and the preparation conditions of heating the alcohol at 110 °C for 48 h were finally determined (Figure S5). Then, the calcination temperature of the catalyst affected the crystal phase structure of TiO<sub>2</sub>, and 450 °C was selected based on the principle of energy saving (Figures S6–S8).

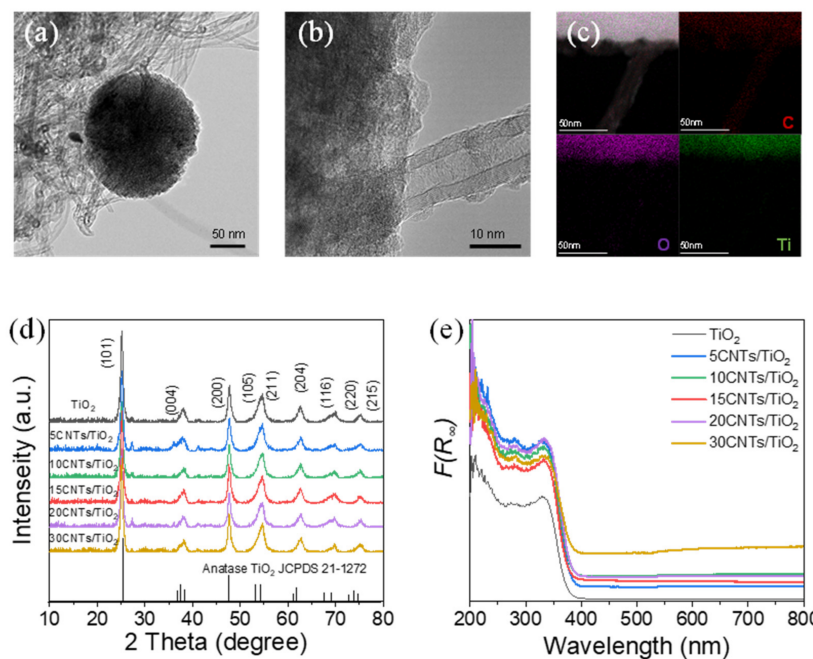


**Figure 1.** (a) TEM image, (b) HADDF-HRTEM image, and (c) EDS elemental mapping of 15CNTs/TiO<sub>2</sub>. (d) X-ray diffraction patterns of pure TiO<sub>2</sub> and xCNTs/TiO<sub>2</sub>. (e) UV-vis diffuse reflectance spectra of TiO<sub>2</sub> and xCNTs/TiO<sub>2</sub>.

In order to visually illustrate the microwave photocatalytic degradation process, we used TiO<sub>2</sub>, CNTs, and 15CNTs/TiO<sub>2</sub> as research objects. From the FT-IR spectra, it can be seen that the broadband consisting of 15CNTs/TiO<sub>2</sub> composed of Ti–O–Ti and Ti–O–C bonds appears at a low wavenumber (660 cm<sup>-1</sup>) (Figure 3a) [29,30]. The peak at 3400 cm<sup>-1</sup> was caused by the physical adsorption of hydroxyl functional groups and water molecules on the surface. In addition, the peaks at around 1712 cm<sup>-1</sup>, 1615 cm<sup>-1</sup>, and 1354 cm<sup>-1</sup> belong to C=O carbonyl, the C=C skeletal vibrational of carbon nanotubes, and C–O carboxyl groups, respectively. The formation of these peaks indicates that the CNTs had good binding to the TiO<sub>2</sub>. As can be seen from the Raman spectroscopy, the peak appearing at 1315 cm<sup>-1</sup> is called the D band, whose intensity corresponds to the degree of lattice defects in the carbon nanotubes. The peak appearing at 1577 cm<sup>-1</sup> is the G band, which corresponds to the characteristic peak of the in-plane stretching vibration of the

$sp_2$  hybridization of the CNTs. The 2D band is associated with Raman scattering due to the vibrational mode characterized by the breathing of six carbons around a hexagon. By comparing the CNTs and 15CNTs/TiO<sub>2</sub>, it was found that the peak positions and peak intensities of both were the same, so the CNT structure in the 15CNTs/TiO<sub>2</sub> was not destroyed and played a good role in the reaction. (Figure 3b). In addition, X-ray photoelectron spectroscopy (XPS) further confirmed the relationship between TiO<sub>2</sub> and CNTs (Figure S9). The detailed Ti 2*p* spectra of the TiO<sub>2</sub> show two symmetric peaks at 459.0 eV and 464.7 eV (Figure 4a), which have been attributed to Ti<sup>4+</sup> [31,32]. Upon binding to the CNTs, the Ti 2*p* and O 1*s* peaks moved toward higher binding energies, which may have been due to the interaction between the TiO<sub>2</sub> and CNTs. The O 1*s* spectrum of the 15CNTs/TiO<sub>2</sub> shows a shoulder peak at 530.2 eV, associated with bridging hydroxyl groups (Figure 4b) [33]. These hydroxyl groups may have been generated by the dissociative adsorption of water on oxygen vacancies, indicating the possible presence of oxygen vacancies. There was no shift in the binding energy position of C in the C 1*s* spectrum, but the encapsulation of the TiO<sub>2</sub> led to a decrease in the intensity of the C peak of the CNTs (Figure 4c).

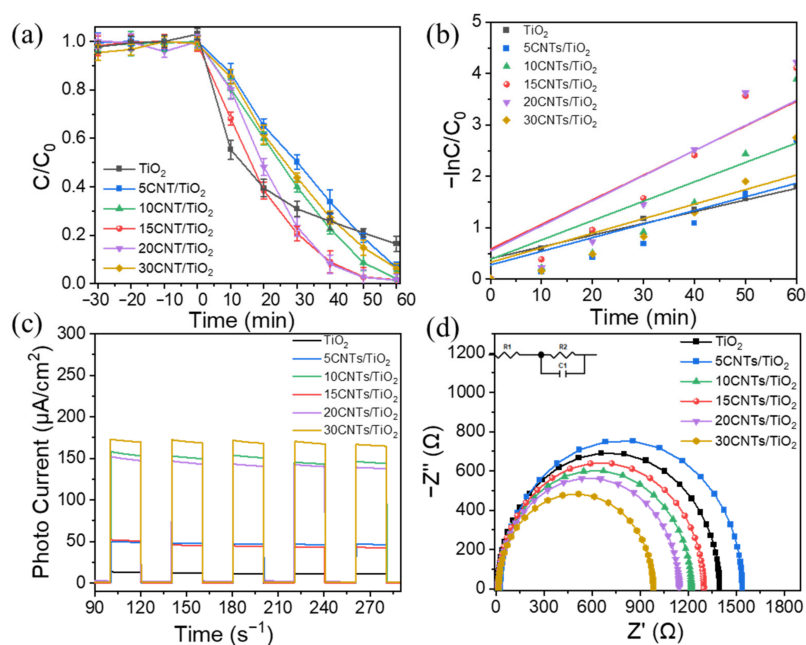


**Figure 2.** (a) The degradation activity of xCNTs/TiO<sub>2</sub> under microwave and UV irradiation; the reaction temperature was 60 °C. (b) The kinetic fitting curve of MO degradation by xCNTs/TiO<sub>2</sub>. (c) Photocurrent spectra of TiO<sub>2</sub> and xCNTs/TiO<sub>2</sub>. (d) Electrochemical impedance spectra of TiO<sub>2</sub> and xCNTs/TiO<sub>2</sub>.

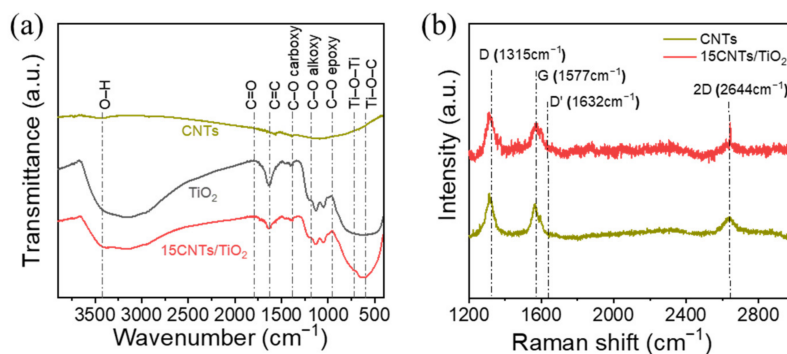


**Figure 3.** (a) The FTIR spectrum of CNTs, TiO<sub>2</sub>, and 15CNTs/TiO<sub>2</sub>. (b) The Raman spectrum of 15CNTs/TiO<sub>2</sub> and CNTs.

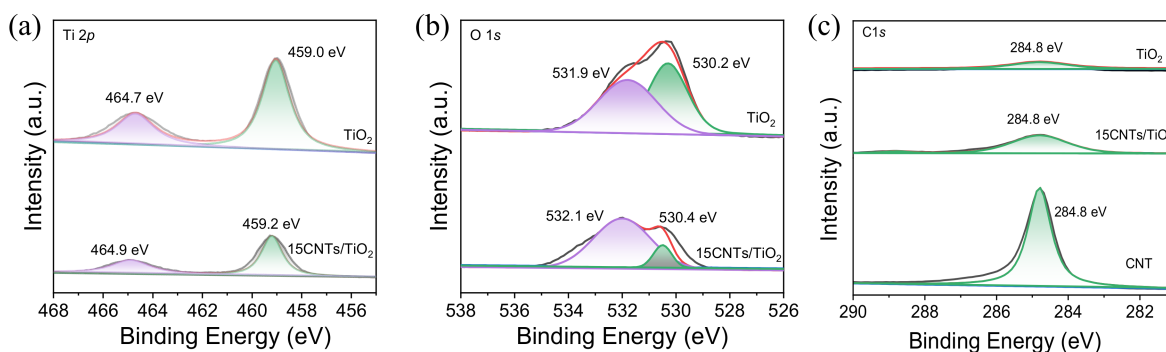


**Figure 4.** The XPS spectra of 15CNTs/TiO<sub>2</sub> and TiO<sub>2</sub>: Ti 2p (a), O 1s, (b) and C 1s (c).

After clarifying the structure of the catalyst, we adjusted the reaction conditions of the degradation process to explore the reaction mechanism of UV and MW. As the microwave power increased, the degradation activity of the MO reached a maximum of 600 W (Figure 5a,b). To distinguish the thermal and non-thermal effects of microwaves and the reaction conditions of traditional heating, only microwave, and only ultraviolet light were set, respectively. In the absence of light, the microwave could not catalyze the degradation of MO, while the photocatalytic degradation efficiency of the MO increased by 1.25 times under the assistance of traditional heating, which indicates that the thermal effect promoted the catalytic process. When the microwave and ultraviolet light were added at the same time, the degradation of MO was 2.5 times higher than that of pure photocatalysis, suggesting an important role of microwave athermal effects (Figure 5c,d). The physicochemical parameters affecting the photodegradation process were further analyzed by quantifying the pollutant concentrations and reaction temperatures. Figure S11a shows that a higher content of CNTs on the catalyst during the degradation of low-concentration MO (10 ppm) led to greater adsorption of the MO, so the microwave photodegradation performance of the catalyst could not be accurately compared. At the higher concentration of MO (40 ppm), the adsorption capacity of different catalysts to pollutants was similar. Among them, 15CNTs/TiO<sub>2</sub> exhibited the best microwave photocatalytic degradation performance, which indicates that the addition of CNTs was beneficial to the degradation of pollutants, but the loading of CNTs was not as high as possible (Figure S10b). The reaction temperature had no great influence on the degradation rate of the MO, and it can be seen that the 15CNTs/TiO<sub>2</sub> had good temperature universality (Figure S10c). Furthermore, the universality of the catalyst was further investigated, and the experimental data show that the RhB degradation efficiency under microwave photocatalysis was 10.7% higher than that under UV conditions alone (Figure S11). The catalyst had good stability, and the complete degradation of the MO was guaranteed in the first three experiments (Figure S12). However, the degradation activity was slightly reduced due to the adsorption of a large amount of organic matter on the catalyst surface. We further used 4-CP, MB, RHB, and other pollutants to simulate the microwave photocatalytic degradation of actual samples and natural environmental conditions, and the results prove that the addition of microwave played a key role in the photocatalytic degradation of the pollutants (Figure S13).

To determine the catalytic degradation mechanism under microwave photocatalysis, we measured the removal rate after the addition of radical trapping agents. The 15CNTs/TiO<sub>2</sub> catalyst efficiently generated e<sup>-</sup>/h<sup>+</sup> pairs in response to UV light [34,35], and the charge separation efficiency was sufficient for the reaction of photogenerated e<sup>-</sup>/h<sup>+</sup> with adsorbed oxygen/H<sub>2</sub>O to generate a series of reactive oxygen radicals. When the hydroxyl radicals (•OH) were trapped, the MO removal rate decreased from 98.3% to 73.8%. After the superoxide radicals (•O<sub>2</sub><sup>-</sup>), holes (h<sup>+</sup>), and electrons (e<sup>-</sup>) were trapped, the MO was almost not degraded (Figure 6a). The signals of DMPO-•O<sub>2</sub><sup>-</sup> and DMPO-•OH were measured using the ESR spin trap technique. As shown in Figure 6b, the six characteristic peaks of the DMPO-•O<sub>2</sub><sup>-</sup> radical sites can be observed. Another four characteristic peaks

of DMPO- $\bullet$ OH also had an evident signal intensity ratio of 1:2:2:1, as shown in Figure 6c, while no such signal was detected in the dark. In conclusion,  $\bullet$ OH,  $\bullet$ O<sub>2</sub><sup>-</sup>, e<sup>-</sup>, and h<sup>+</sup> all had a positive effect on the reaction.

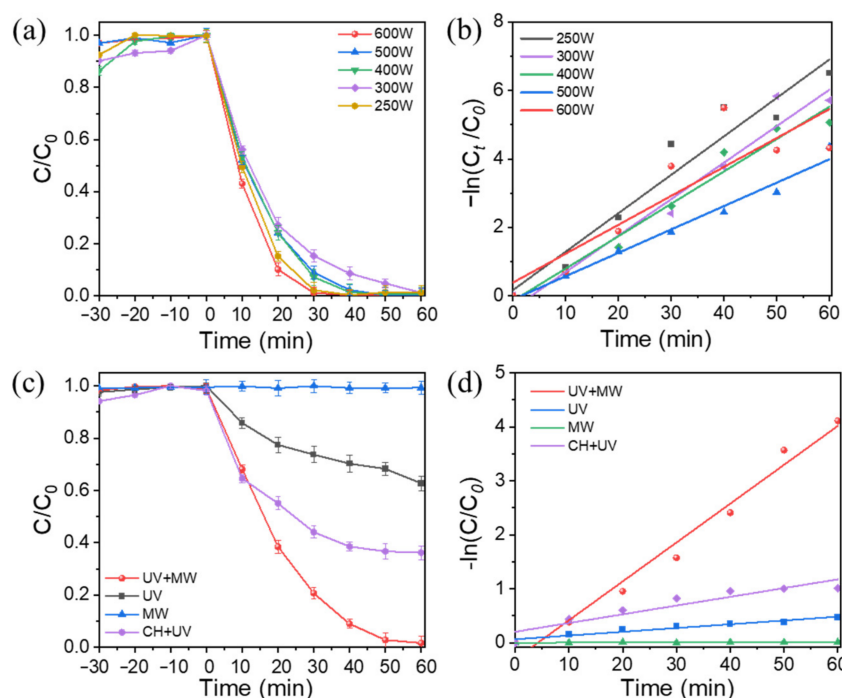


**Figure 5.** (a) The degradation activity and (b) the kinetics fitting curve of 15CNTs/TiO<sub>2</sub> under UV with different power microwave irradiation. (c) The degradation activity and (d) the kinetics fitting curve of 15CNTs/TiO<sub>2</sub> under different conditions.

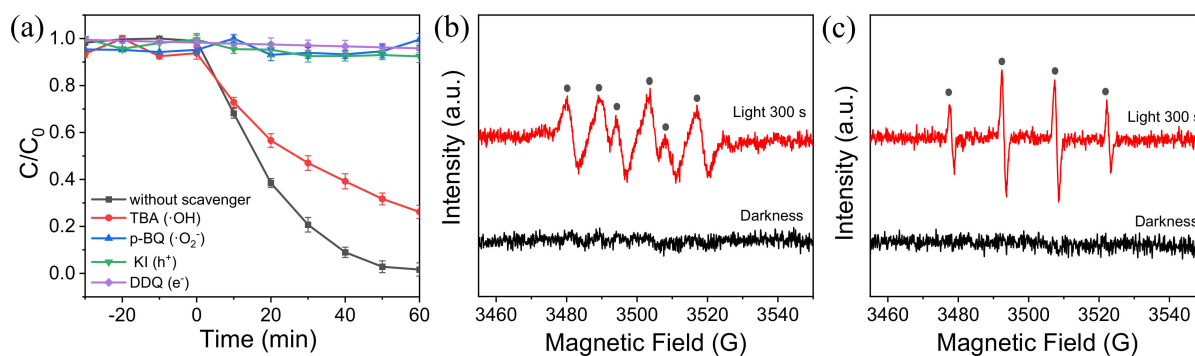


**Figure 6.** (a) Active species capture experiment of 15CNTs/TiO<sub>2</sub> for MO degradation under microwave and UV irradiation. The EPR spectra of free radicals using 15CNTs/TiO<sub>2</sub>:  $\bullet$ O<sub>2</sub><sup>-</sup> (b) and  $\bullet$ OH (c).

In general, photocatalytic advanced oxidation processes can efficiently mineralize organic pollutants into water and carbon dioxide [36,37]. In this work, hot spots and defects were formed on the catalyst surface under the thermal effect of microwaves to capture photogenerated electrons and improve the separation efficiency of the photogenerated carriers (Figure 7). The athermal effect of the microwave field had a polarizing effect on the catalyst, which improved the light absorption rate of the catalyst and promoted the activation of oxygen molecules and hydroxyl groups on the surface of the catalyst, generating more active oxygen radicals ( $\bullet$ O<sub>2</sub><sup>-</sup> and  $\bullet$ OH) for the degradation of pollutants. It follows that the TiO<sub>2</sub> generated electron-hole pairs under UV light irradiation, and the generated electrons were immediately transferred from the TiO<sub>2</sub> to the CNT surfaces through the mutual bridging between the CNT/TiO<sub>2</sub> interfaces, which effectively reduced the com-

pound rate of the  $e^-/h^+$ . The separated  $e^-/h^+$  drove the redox reaction in an aqueous solution. The  $h^+$  oxidized the water to form  $\bullet OH$ , and the  $e^-$  that were transferred to the carbon nanotubes reacted with the  $O_2$  to induce the reduction of oxygen to  $\bullet O_2^-$  [38,39]. In the process, the unique structures of the CNTs not only improved the ability to capture light but also absorbed the energy generated by the microwaves and converted it into heat energy. At the interface with  $TiO_2$ , the CNTs generated local super-hot spots to accelerate the mobility of photogenerated carriers, and finally achieved the purpose of improving the photocatalytic efficiency.

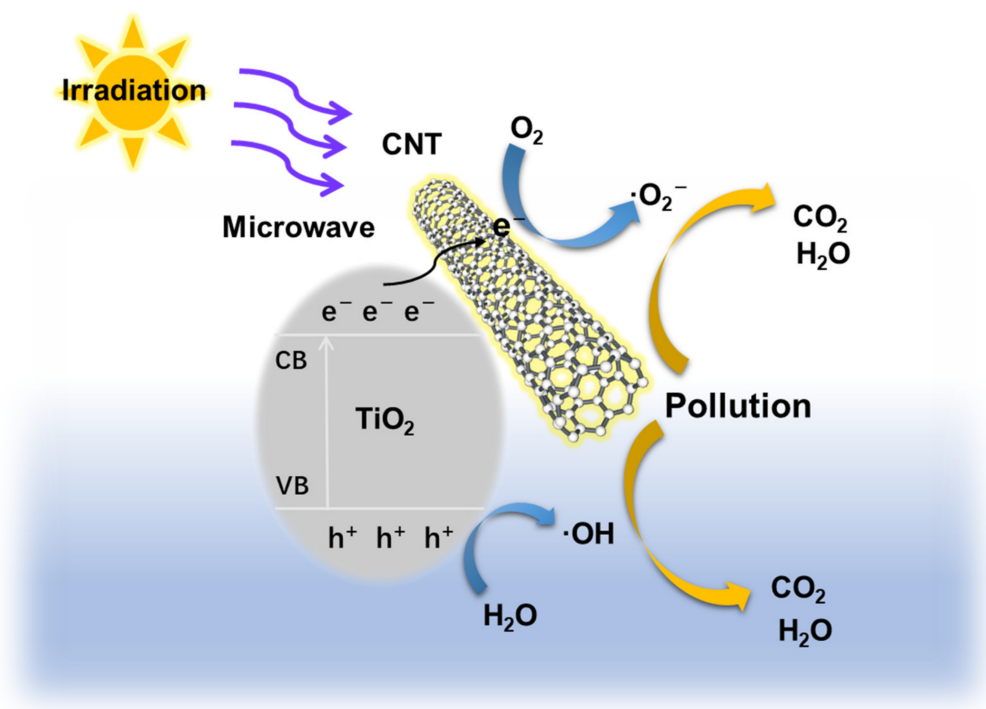


**Figure 7.** Schematic of CNTs/ $TiO_2$  catalyst for pollutant degradation.

### 3. Materials and Methods

#### 3.1. Materials

All chemicals used in this study were of analytical grade and were not further purified: carbon nanotubes (CNTs, Aladdin,  $\geq 95\%$ ), methyl orange (MO, Aladdin, AR,  $\geq 95\%$ ), rhodamine B (RhB, Aladdin, AR,  $\geq 95\%$ ), titanium oxide (commercial sample of Degussa P-25), ethanol ( $C_2H_5OH$ , Aladdin, AR, 99%), methanol ( $CH_3OH$ , J&K, AR, 99%), titanium (IV) oxide sulfate sulfuric acid hydrate ( $TiOSO_4$ , Aladdin, AR, 99%), potassium iodide (KI, J&K, AR, 99%); tert-butanol (TBA, Adamas, AR, 99%), p-benzoquinone (p-BQ, Aladdin, AR, 99%), and 2,3-dichloro-5,6-dicyano-p-benzoquinone (DDQ, Aladdin, AR, 99%). All of the chemicals were used as received.

#### 3.2. Preparation of Catalysts

##### 3.2.1. Preparation of xCNTs/ $TiO_2$ Using the Alcoholic Thermal Method

The catalysts used in this study were prepared using the alcoholic heat method. At room temperature, the appropriate amount of CNTs (20–30 nm in diameter) was completely submerged in 3.0 mL of anhydrous ethanol and then dispersed until homogeneous using ultrasonication. Then, 3.0 mL of titanium oxide sulfate and 50 mL of tert-butanol were added, respectively. The mixtures were stirred until completely mixed uniformly, and then they were transferred to a hydrothermal kettle and reacted in an oven at  $110\text{ }^\circ\text{C}$  for 48 h. The reaction product was washed several times with ethanol, dried at  $80\text{ }^\circ\text{C}$ , and ground and the obtained materials were named xCNTs/ $TiO_2$  according to the different doping contents of the CNTs.

### 3.2.2. Preparation of TiO<sub>2</sub> Using the Alcoholic Thermal Method

At room temperature, 3.0 mL of titanium oxide sulfate was added to 3.0 mL of anhydrous ethanol, and 50 mL of tert-butanol was added while stirring. After stirring for 1 h, the mixture was completely mixed, transferred to the PTFE liner, and reacted in an oven at 110 °C for 48 h. The reaction product was washed several times with alcohol, then dried and ground at 80 °C. The resulting material was calcined in air for 2 h, and the resulting powdered sample was named TiO<sub>2</sub>.

### 3.3. Characterization

The powdered sample was characterized using X-ray diffraction (XRD, Rigaku D/MAX-2000, Rigaku, Tokyo, Japan) with a Cu K $\alpha$  source at 40 kV, 20 mA (scan rate: 10 min<sup>-1</sup>), X-ray photoelectron spectroscopy (XPS, PerkinElmer PHI 5000C, Al K $\alpha$ , Perkin Elmer, Tokyo, Japan), Nicolet iS10 Fourier (Thermo Fisher Scientific, Waltham, MA, USA) transform infrared spectrometer (FT-IR), and UV-vis diffuse reflectance spectra (Shimadzu, UV2600, Tokyo, Japan) in the range of 200–800 nm, using BaSO<sub>4</sub> as the reflectance standard. The UV-7502 liquid UV spectrophotometer (Xinmao, Shanghai, China) was used for the quantitative and qualitative analysis of organic residues during the activity test. The morphology was characterized using a scanning electron microscope (SEM, Hitachi S4800, JEOL, Tokyo, Japan) and a transmission electron microscope (TEM, JEOL JEM-2010, 200 kV operation, JEOL, Tokyo, Japan). A JES FA200 (JEOL, Tokyo, Japan) electron paramagnetic resonance spectrometer was used to test the free radical species generated during the reaction.

### 3.4. Activity Test

The photocatalytic degradation performance of the synthesized catalysts was tested using the photodegradation of the methyl orange (MO) and rhodamine B (RhB) aqueous solutions. For the test, 40 mg of catalyst was dispersed in 40 mL of MO (or RhB) contaminant aqueous solution (20 mg/L). Before the light reaction, the mixture was placed in the dark and under no microwave conditions for 30 min to test the adsorption capacity of the catalyst to pollutants. The reaction solution was then placed in a special microwave photocatalytic reactor (UWave-2000 Multifunctional Microwave Synthesis Extractor consisting of a 2.45 GHz microwave generator (maximum power 1.0 kW, Science Laboratories, Shanghai, China) and a built-in UV lamp (300 W, mercury lamp)) to start the degradation experiment. A 1 mL sample was taken every 10 min, and the supernatant was taken after centrifugation to determine the residual concentration of pollutants in a UV-vis spectrophotometer (UV-7502, Xinmao, Shanghai, China). According to the needs of the experiment, the reaction conditions were adjusted to complete the control group experiment. Since the microwave reaction caused the temperature of the system itself to rise, we set the temperature of the heating control to the same temperature (60 °C) as the microwave irradiation.

### 3.5. Photoelectrochemical Measurements

All photoelectrochemical measurements were performed at room temperature, using the electrochemical analyzer (CHI 660E electrochemical station, Chenhua, Shanghai, China) with a single-chamber quartz cell and a standard three-electrode system. Indium-doped tin oxide (ITO) substrates were ultrasonically cleaned in deionized water, anhydrous ethanol, and isopropanol for 30 min. The deionized water-dispersed samples slurry were spread on the ITO glass substrates. The spread film was dried in air and annealed at 150 °C for 10 min. In a standard three-electrode system, a platinum sheet (10 mm  $\times$  20 mm) was used as the counter electrode, a saturated glycogen reference electrode (SCE), and a thin-film working electrode for different catalysts; all three electrodes were placed in a quartz cell. The photocurrent test procedure used a 365 nm LED lamp as the light source and an aqueous Na<sub>2</sub>SO<sub>4</sub> solution (0.50 M) as the electrolyte. The variation in the photocurrent with response time was explored using the modulation of the lamp switching process.

### 3.6. Radical-Trapping Experiment

The p-benzoquinone (p-BQ), potassium iodide (KI), tert-butanol (TBA), and 2,3-dichloro-5,6-dicyano-1,4-benzoquinone (DDQ) were used as scavengers for the superoxide radicals ( $\bullet\text{O}_2^-$ ), holes ( $\text{h}^+$ ), hydroxyl radicals ( $\bullet\text{OH}$ ), and electrons ( $\text{e}^-$ ), respectively. Similar to the measurement of microwave photocatalytic activity, 40 mg of catalyst was dispersed in 40 mL of an aqueous solution of methyl orange contaminant (20 mg/L), with 1 mM of trapping agent. The mixture was stirred in the dark for 30 min to achieve adsorption equilibrium between the catalyst and the solution. After irradiation, the suspension was collected every 10 min, and then the concentration of MO was measured using a UV-vis spectrophotometer (UV-7502).

## 4. Conclusions

In summary, a typical microwave photocatalyst, CNTs/TiO<sub>2</sub>, was constructed using a simple thermal method, which efficiently mineralized organic pollutants with the assistance of microwave fields. By modulating the reaction conditions, the active mode of the thermal effect and athermal effect brought by the microwave field was clarified in the photocatalytic oxidation process. The thermal effect quickly formed a large number of hot spots on the surfaces of the CNTs and promoted the desorption of small molecules after degradation. Meanwhile, the athermal effect not only polarized the CNTs/TiO<sub>2</sub> but also accelerated the activation of oxygen groups on the surfaces of the CNTs/TiO<sub>2</sub>. The  $\text{h}^+$  oxidized water and hydroxide ions to form  $\bullet\text{OH}$ , and the  $\text{e}^-$  transferred CNTs reacted with O<sub>2</sub> to induce oxygen reduction to  $\bullet\text{O}_2^-$ . These reactive intermediates worked together to accelerate the degradation of the pollutants. Based on this in-depth exploration of the microwave effect, a new perspective is provided for the study of the mechanism of the microwave photocatalytic reaction.

**Supplementary Materials:** The following supporting information can be downloaded at: <https://www.mdpi.com/article/10.3390/catal12090940/s1>, Figure S1: SEM image of (a) CNTs and (b) acidified CNTs (ACNTs). Figure S2: FTIR spectra of CNTs and ACNTs. Figure S3: Raman spectrum of CNTs and ACNTs. Figure S4: SEM images of TiO<sub>2</sub> (a,b), 5CNTs/TiO<sub>2</sub> (c,d), 10CNTs/TiO<sub>2</sub> (e,f), 15CNTs/TiO<sub>2</sub> (g,h), 20CNTs/TiO<sub>2</sub> (i,j), and 30CNTs/TiO<sub>2</sub> (k,l). Figure S5: (a) Degradation activity of different 15CNTs/TiO<sub>2</sub> under microwave and UV irradiation for 1 h. (b) Degradation activity of different 15CNTs/TiO<sub>2</sub> under microwave and UV irradiation for 1 h. Figure S6: XRD spectra of 15CNTs/TiO<sub>2</sub> calcined at different temperatures. Figure S7: Photographs of 15CNTs/TiO<sub>2</sub> calcined at different temperatures. Figure S8: Degradation activity of 15CNTs/TiO<sub>2</sub> calcined at different temperatures. Figure S9: XPS spectra of 15CNTs/TiO<sub>2</sub> (a) and TiO<sub>2</sub> (b). Figure S10: (a) Activity data of different catalysts for the degradation of MO at 10 ppm. (b) Activity data of different catalysts for the degradation of MO at 40 ppm. (c) Effects of different temperatures on the reactivity of degraded MO. Figure S11: (a) RhB degradation activity of 15CNTs/TiO<sub>2</sub> under different conditions. The UV-vis spectra of RhB degraded by 15CNTs/TiO<sub>2</sub> at different times under (b) ultraviolet alone (UV) and (c) UV illumination and microwave radiation conditions. Figure S12: Recycling test of 15CNTs/TiO<sub>2</sub> for MO degradation under microwave and UV irradiation. Figure S13: The microwave photocatalytic degradation of 4-CP, MB, and RhB by 15CNTs/TiO<sub>2</sub>.

**Author Contributions:** Y.R., Y.C. and Q.L. contributed equally to this work. Conceptualization, Y.R. and Y.C.; methodology, Q.L.; writing—original draft preparation, Y.C. and Q.L.; writing—review and editing, Y.R. and Y.C.; supervision, H.L. and Z.B.; funding acquisition, H.L. and Z.B. All authors have read and agreed to the published version of the manuscript.

**Funding:** This work was supported by the National Key Research and Development Program of China (2020YFA0211004), the National Natural Science Foundation of China (22176128,21876114), Shanghai Government (21XD1422800,19DZ1205102, and 19160712900), the Chinese Education Ministry Key Laboratory and International Joint Laboratory on Resource Chemistry, the Shanghai Eastern Scholar Program, the Shanghai Engineering Research Center of Green Energy Chemical Engineering (18DZ2254200), and the Shanghai Frontiers Science Center of Biomimetic Catalysis.

**Data Availability Statement:** Data supporting the research are available upon reasonable request.

**Acknowledgments:** Thanks for the technical support from the MOE Key Laboratory of Resource Chemistry and the Shanghai Key Laboratory of Rare Earth Functional Materials, Shanghai Normal University.

**Conflicts of Interest:** The authors declare no conflict of interest.

## References

1. Fiorenza, R.; Di Mauro, A.; Cantarella, M.; Iaria, C.; Scalisi, E.M.; Brundo, M.V.; Gulino, A.; Spitaleri, L.; Nicotra, G.; Dattilo, S.; et al. Preferential removal of pesticides from water by molecular imprinting on TiO<sub>2</sub> photocatalysts. *Chem. Eng. J.* **2020**, *379*, 122309. [[CrossRef](#)]
2. Arthur, R.B.; Bonin, J.L.; Ardill, L.P.; Rourk, E.J.; Patterson, H.H.; Stemmler, E.A. Photocatalytic degradation of ibuprofen over BiOCl nanosheets with identification of intermediates. *J. Hazard. Mater.* **2018**, *358*, 1–9. [[CrossRef](#)]
3. Zhang, Z.; Liang, Y.; Huang, H.; Liu, X.; Li, Q.; Chen, L.; Xu, D. Stable and Highly Efficient Photocatalysis with Lead-Free Double-Perovskite of Cs<sub>2</sub>AgBiBr<sub>6</sub>. *Angew. Chem. Int. Ed.* **2019**, *58*, 7263–7267. [[CrossRef](#)] [[PubMed](#)]
4. Guo, Q.; Sun, D.-W.; Cheng, J.-H.; Han, Z. Microwave processing techniques and their recent applications in the food industry. *Trends Food. Sci. Technol.* **2017**, *67*, 236–247. [[CrossRef](#)]
5. Green, M.; Liu, Z.; Xiang, P.; Liu, Y.; Zhou, M.; Tan, X.; Huang, F.; Liu, L.; Chen, X. Doped, conductive SiO<sub>2</sub> nanoparticles for large microwave absorption. *Light Sci. Appl.* **2018**, *7*, 87. [[CrossRef](#)] [[PubMed](#)]
6. Iguchi, Y.; Nii, Y.; Onose, Y. Magnetolectrical control of nonreciprocal microwave response in a multiferroic helimagnet. *Nat. Commun.* **2017**, *8*, 15252. [[CrossRef](#)]
7. El Khaled, D.; Novas, N.; Gazquez, J.A.; Manzano-Agugliaro, F. Microwave dielectric heating: Applications on metals processing. *Renew. Sust. Energy. Rev.* **2018**, *82*, 2880–2892. [[CrossRef](#)]
8. Xiao, S.; Dai, W.; Liu, X.; Pan, D.; Zou, H.; Li, G.; Zhang, G.; Su, C.; Zhang, D.; Chen, W.; et al. Microwave-Induced Metal Dissolution Synthesis of Core-Shell Copper Nanowires/ZnS for Visible Light Photocatalytic H<sub>2</sub> Evolution. *Adv. Energy Mater.* **2019**, *9*, 1900775. [[CrossRef](#)]
9. Xiao, S.; Zhang, D.; Pan, D.; Zhu, W.; Liu, P.; Cai, Y.; Li, G.; Li, H. A chloroplast structured photocatalyst enabled by microwave synthesis. *Nat. Commun.* **2019**, *10*, 1570. [[CrossRef](#)]
10. Hussain, H.; Tocci, G.; Woolcot, T.; Torrelles, X.; Pang, C.L.; Humphrey, D.S.; Yim, C.M.; Grinter, D.C.; Cabailh, G.; Bikondoa, O.; et al. Structure of a model TiO<sub>2</sub> photocatalytic interface. *Nat. Mater.* **2017**, *16*, 461–466. [[CrossRef](#)]
11. Gole, V.L.; Priya, A. Microwave-photocatalyzed assisted degradation of brilliant green dye: A batch to continuous approach. *J. Water Process. Eng.* **2017**, *19*, 101–105. [[CrossRef](#)]
12. Barik, A.J.; Kulkarni, S.V.; Gogate, P.R. Degradation of 4-chloro 2-aminophenol using combined approaches based on microwave and photocatalysis. *Sep. Purif.* **2016**, *168*, 152–160. [[CrossRef](#)]
13. Nguyen, K.C.; Ngoc, M.P.; Nguyen, M.V. Enhanced photocatalytic activity of nanohybrids TiO<sub>2</sub>/CNTs materials. *Mater. Lett.* **2016**, *165*, 247–251. [[CrossRef](#)]
14. Guo, Q.; Zhou, C.; Ma, Z.; Ren, Z.; Fan, H.; Yang, X. Elementary photocatalytic chemistry on TiO<sub>2</sub> surfaces. *Chem. Soc. Rev.* **2016**, *45*, 3701–3730. [[CrossRef](#)]
15. Fujishima, A.; Honda, K. Electrochemical Photolysis of Water at a Semiconductor Electrode. *Nature* **1972**, *238*, 37–38. [[CrossRef](#)]
16. Selcuk, S.; Selloni, A. Facet-dependent trapping and dynamics of excess electrons at anatase TiO<sub>2</sub> surfaces and aqueous interfaces. *Nat. Mater.* **2016**, *15*, 1107–1112. [[CrossRef](#)]
17. Zhang, W.; He, H.; Tian, Y.; Lan, K.; Liu, Q.; Wang, C.; Liu, Y.; Elzatahry, A.; Che, R.; Li, W.; et al. Synthesis of uniform ordered mesoporous TiO<sub>2</sub> microspheres with controllable phase junctions for efficient solar water splitting. *Chem. Sci.* **2019**, *10*, 1664–1670. [[CrossRef](#)]
18. Naldoni, A.; Altomare, M.; Zoppellaro, G.; Liu, N.; Kment, S.; Zboril, R.; Schmuki, P. Photocatalysis with Reduced TiO<sub>2</sub>: From Black TiO<sub>2</sub> to Cocatalyst-Free Hydrogen Production. *ACS Catal.* **2019**, *9*, 345–364. [[CrossRef](#)]
19. Pu, S.; Zhu, R.; Ma, H.; Deng, D.; Pei, X.; Qi, F.; Chu, W. Facile in-situ design strategy to disperse TiO<sub>2</sub> nanoparticles on graphene for the enhanced photocatalytic degradation of rhodamine 6G. *Appl. Catal. B* **2017**, *218*, 208–219. [[CrossRef](#)]
20. Zhang, K.; Li, D.; Cao, H.; Zhu, Q.; Trapalis, C.; Zhu, P.; Gao, X.; Wang, C. Insights into different dimensional MXenes for photocatalysis. *Chem. Eng. J.* **2021**, *424*, 130340. [[CrossRef](#)]
21. Li, L.; Wang, X.S.; Liu, T.F.; Ye, J. Titanium-Based MOF Materials: From Crystal Engineering to Photocatalysis. *Small Methods* **2020**, *4*, 2000486. [[CrossRef](#)]
22. Yu, J.; Ma, T.; Liu, S. Enhanced photocatalytic activity of mesoporous TiO<sub>2</sub> aggregates by embedding carbon nanotubes as electron-transfer channel. *Phys. Chem. Chem. Phys.* **2011**, *13*, 3491–3501. [[CrossRef](#)]
23. Wen, B.; Cao, M.; Lu, M.; Cao, W.; Shi, H.; Liu, J.; Wang, X.; Jin, H.; Fang, X.; Wang, W.; et al. Reduced graphene oxides: Light-weight and high-efficiency electromagnetic interference shielding at elevated temperatures. *Adv. Mater.* **2014**, *26*, 3484–3489. [[CrossRef](#)]
24. Cao, M.-S.; Song, W.-L.; Hou, Z.-L.; Wen, B.; Yuan, J. The effects of temperature and frequency on the dielectric properties, electromagnetic interference shielding and microwave-absorption of short carbon fiber/silica composites. *Carbon* **2010**, *48*, 788–796. [[CrossRef](#)]

25. Nanda Sahoo, B.; Choi, B.; Seo, J.; Lee, T. Hybrid functional microfibers for textile electronics and biosensors. *J. Semicond.* **2018**, *39*, 011009. [[CrossRef](#)]
26. Chen, J.; Xue, S.; Song, Y.; Shen, M.; Zhang, Z.; Yuan, T.; Tian, F.; Dionysiou, D.D. Microwave-induced carbon nanotubes catalytic degradation of organic pollutants in aqueous solution. *J. Hazard. Mater.* **2016**, *310*, 226–234. [[CrossRef](#)]
27. Guaglianoni, W.C.; Florence, C.L.; Bonatto, F.; Venturini, J.; Arcaro, S.; Alves, A.K.; Bergmann, C.P. Novel nanoarchitected cobalt-doped TiO<sub>2</sub> and carbon nanotube arrays: Synthesis and photocurrent performance. *Ceram. Int.* **2019**, *45*, 2439–2445. [[CrossRef](#)]
28. Luo, W.; Hou, J.-L.; Zou, D.-H.; Cui, L.-N.; Zhu, Q.-Y.; Dai, J. Lanthanide–titanium-oxalate clusters and their degradation products, photocurrent response and photocatalytic behaviours. *New J. Chem.* **2018**, *42*, 11629–11634. [[CrossRef](#)]
29. Darvishi, M.; Seyed-Yazdi, J. Effect of microwave power on created defects in graphene sheet of synthesized TiO<sub>2</sub>/graphene nanocomposite with enhanced photocatalytic performance. *Surf. Interfaces* **2016**, *4*, 1–8. [[CrossRef](#)]
30. Xu, Y.; Bai, H.; Lu, G.; Li, C.; Shi, G. Flexible Graphene Films via the Filtration of Water-Soluble Noncovalent Functionalized Graphene Sheets. *J. Am. Chem. Soc.* **2008**, *130*, 5856–5857. [[CrossRef](#)]
31. Wu, X.; Chen, Z.; Lu, G.Q.M.; Wang, L. Nanosized Anatase TiO<sub>2</sub> Single Crystals with Tunable Exposed (001) Facets for Enhanced Energy Conversion Efficiency of Dye-Sensitized Solar Cells. *Adv. Funct. Mater.* **2011**, *21*, 4167–4172. [[CrossRef](#)]
32. Liu, Z.; Zheng, Y.; Gao, T.; Zhang, J.; Sun, X.; Zhou, G. Fabrication of anatase TiO<sub>2</sub> tapered tetragonal nanorods with designed {100}, {001} and {101} facets for enhanced photocatalytic H<sub>2</sub> evolution. *Int. J. Hydrogen Energy* **2017**, *42*, 21775–21785. [[CrossRef](#)]
33. Wang, G.; Yue, F.; Zhang, L.; Yan, B.; Luo, J.; Su, X. Oxygen vacancy-rich anatase TiO<sub>2</sub> hollow spheres via liquid nitrogen quenching process for enhanced photocatalytic hydrogen evolution. *Chem. Cat. Chem.* **2018**, *11*, 1043–1057. [[CrossRef](#)]
34. Gao, B.; Chen, G.Z.; Li Puma, G. Carbon nanotubes/titanium dioxide (CNTs/TiO<sub>2</sub>) nanocomposites prepared by conventional and novel surfactant wrapping sol–gel methods exhibiting enhanced photocatalytic activity. *Appl. Catal. B Environ.* **2009**, *89*, 503–509. [[CrossRef](#)]
35. Yu, H.; Quan, X.; Chen, S.; Zhao, H. TiO<sub>2</sub>-Multiwalled Carbon Nanotube Heterojunction Arrays and Their Charge Separation Capability. *J. Phys. Chem. C* **2007**, *111*, 12987–12991. [[CrossRef](#)]
36. Bahrudin, N.N.; Nawi, M.A. Mechanistic of photocatalytic decolorization and mineralization of methyl orange dye by immobilized TiO<sub>2</sub>/chitosan-montmorillonite. *J. Water Process. Eng.* **2019**, *31*, 100843. [[CrossRef](#)]
37. Chang, Z.Y.; Wang, Z.Y.; Zhang, R.; Yu, L. Acceleration of biotic decolorization and partial mineralization of methyl orange by a photo-assisted n-type semiconductor. *Chemosphere* **2022**, *291*, 132846. [[CrossRef](#)]
38. Nosaka, Y.; Nosaka, A.Y. Generation and Detection of Reactive Oxygen Species in Photocatalysis. *Chem. Rev.* **2017**, *117*, 11302–11336. [[CrossRef](#)]
39. Zhang, L.; Mohamed, H.H.; Dillert, R.; Bahnemann, D. Kinetics and mechanisms of charge transfer processes in photocatalytic systems: A review. *J. Photochem. Photobiol. C* **2012**, *13*, 263–276. [[CrossRef](#)]